Chapter 4. Non-thermal and thermal processes

4.1 Coulomb explosion and phase explosion

In the preceding chapters it was suggested that in the initial stages of the ultrashort pulsed laser ablation process of dielectrics an electrostatic mechanism could be the origin of ion emission. The magnitude of this mechanism is determined by photoelectron emission from the surface and the corresponding amount of surface charging inducing the lattice instability. Ions are expelled by the electrostatic interaction with their neighbors and accelerated in the charge-induced electric field.

Arguments for a Coulombic repulsion in UV, ns laser irradiated dielectrics (MgO) in a pre-breakdown, desorption regime have been presented by Dickinson et al. [DLS94] from localized Mg^{+} and Mg^{2+} sites in interaction with ionized *F*-centers but the authors have disregarded the influence of the surface charging in this low fluence regime. Itoh et al. have also suggested localized Coulombic ejection of surface atoms from dielectrics due to the cooperative effects amongst holes in the electron-hole induced plasma and localization on surface adatoms [ItN82].

Sapphire has been extensively investigated with ns pulses due to its many useful mechanical, optical and electrical properties [RoK84, RoKo84, DKW86]. Results have been reported on the quality of the ablation structures [RoK84, TBC89], the optical emission from the ablation plume [DKW86], the energy deposition at the surface [DDG87], and the threshold fluence for laser ablation [DKW86, RoKo84]. Non-thermal mechanisms have been proposed for material removal in the case of ns excimer (248 nm) laser ablation of Al_2O_3 by Dreyfus et al. [DKW86] based on the observation of high translational temperatures for AlO molecules compared to their rotational and vibrational temperatures in the ablation plume. Laser induced plasma threshold measurements in Al_2O_3 compared to metallic aluminium (Al) by Rothenberg et al. [RoKo84] have completed these observations providing evidence of thermal influences for the metallic sample. Nevertheless, even if not clearly seen in the energy spectrum of the ablation products and in their kinetics, a thermal stress loading of the sample (dielectric or metal) is to be expected [Mat97, SFR95]. Ultrashort lasers have the advantage of minimizing the heat diffusion so the thermal load is correspondingly reduced [SFR96].

In the desorption regime excitonic intermediated expulsion via antibonding states has been postulated by Schildbach et al.[ScH92] based on the kinetic energy of the desorbed Al^+ ions which stabilize at a value of 7 eV, independent of the laser fluence.

At higher fluences stress load in the material has been observed [RoK84].

As was shown in Chapter 3, ultrashort pulse laser ablation of dielectrics presents the very characteristic behavior of a two phase appearance, a behavior which is very different from what is known with ns laser irradiation. The transition between the gentle and the strong phase is governed by the number of laser pulses on the same site and depends on the laser intensity.

This chapter will present powerful arguments for a non-thermal, repulsive positive ion ejection from a *macroscopic* affected zone (where significant charge is accumulated) for femtosecond laser ablation and the circumstances necessary for the transition to a thermal mechanism. “Thermal” in this context indicates a process that can be directly associated with a certain temperature (when an equilibrium temperature parameter can be defined for the systems under investigation) or is the consequence of temperature increase. Another aspect of a “thermal” definition will be given in the next chapter based on energy relaxation times in the material.

The investigations presented in this chapter are *in-situ* measurements of the ablation products, adding to the *ex-situ* exploration detailed in Chapter 3.

The present chapter will also analyze the influence of the laser parameters on the ablation process and the conditions for a clean processing of the materials.

Similarities with ion sputtering:

Coulomb explosion was proposed to be the main cause of surface damage and material removal in sputtering of materials with highly charged ions [ScB96], [ChG97]. Experimental evidence has been accumulating that this method may have technological significance for modifying or etching semiconductor or insulator surfaces on a nanometer scale [ScB96, LDS94, Hug95, IMS95].

There is growing interest in the comparison between material modifications induced by ultrashort pulsed lasers and energetic ion beams [CKM97]. This is partly due to the increasing availability of relatively compact, intense, ultrashort pulse laser systems that can be used to couple large amounts of energy into the target on a femtosecond timescale, comparable to the situation with energetic ion bombardment. Laser irradiation differs from the latter in that the thermal effects are more important, although greatly reduced for ultrashort pulses.

Up to now there is very little concrete experimental information about the Coulomb explosion process [ScB96, Mar97]. The main experimental evidence used to justify an explanation in terms of Coulomb explosion is an increase in secondary ion emission and a charge state dependent kinetic energy observed in collisions with very highly charged ions with charge up to 70+ [ScB96].

Recent molecular dynamics (MD) simulations of ion induced Coulomb explosions on silicon surfaces have shown that this mechanism can lead to the production of nanometer scale structures on the surface that are at least in qualitative agreement with what is seen experimentally in highly charged ion-surface collisions (q>40+, typically) [ChG97]. Employing ultrashort pulsed lasers may significantly simplify the process of understanding the basics of the interaction between energetic beams and matter due to the following factors:

- their simplicity in use and manipulation, superior to the highly charged ion sources
- possibility of time resolved dynamic measurements using fs laser pump-probe techniques

The results of the modeling of ion bombardment for silicon targets show many similarities with the results of the simulations of ultrashort pulse laser ablation of silicon for fs pulse durations [HGC97, HGC98]. Both calculations showed an initially fast, explosive (100 fs-1 ps) removal of positive ions due to Coulomb repulsion from the surface followed by relaxation of the target and subsequent ballistic and thermal removal of neutral particles on the ps timescale. It should, however, be mentioned that the MD simulations employ relatively simple phenomenological potentials and are certainly not able to accurately treat the dynamics of the electronically excited states. These studies also do not take account of the electron transport in the irradiated zone. They should thus be regarded as a qualitative indication of the dynamical effects that might be expected to occur in both highly charged ion and ultrashort pulse laser sputtering. Ultrashort pulse laser ablation studies may provide an accessible way of obtaining detailed information on the mechanisms leading to particle emission and could be an important addition to the experimental methods presently applied to explore the role of Coulomb explosion in the nanostructuring of insulator and semiconductor surfaces.

Time-of-flight studies

Ion, electron and neutral time-of-flight techniques have been used to investigate the ablation process as a function of the parameters that are responsible for the different ablation phases and the corresponding mechanisms: fluence (F), pulse duration (τ) and the number of pulses per site (N). While the neutrals carry information mainly related to the surface temperature, ion detection is sensitive to the influence of non-thermal mechanisms.

It will be shown that these are very powerful techniques for obtaining insight into the fundamental mechanisms involved in laser sputtering and suggested that the results are also relevant to understanding the processes involved in sputtering with highly charged ions. The main similarities appear especially in evidence for fast, non-thermal processes such as those discussed in this section. Ultrashort pulsed lasers have proved to be an optimal tool for research in this direction [SAR99, SARW2000]. The secondary effects that concealed much of the fundamental physical processes occurring for laser ablation with standard ns pulsed lasers such as the laser plume interaction and laser heating of the ablated material [Bau96] can be avoided with ultrashort pulses. This is beginning to open the way to a more detailed understanding of the laser-material interactions and mechanisms of material removal [CAR99].

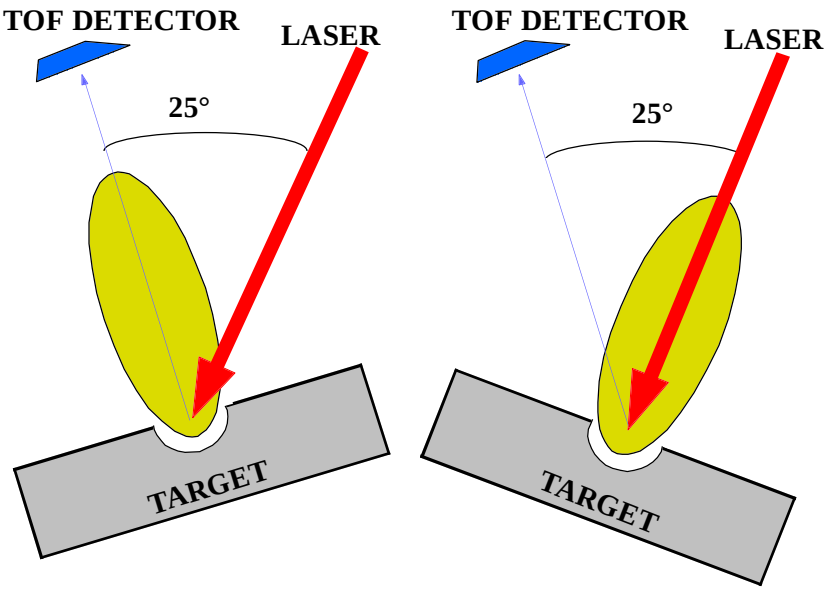

Fig. 4.1-1 TOF detection geometries:
Mode 1: laser at 25° incidence to the sample, TOF detector axis normal to the surface (on-axis detection-left).
Mode 2: laser normal to the sample, TOF detector axis at 25° with respect to the surface normal (off-axis detection-right).

To obtain information about the velocity range of the emitted particles two geometries have been used (see Chapter 2). These are depicted in Fig. 4.1-1. The reason for employing different geometries was the following. The intention was to quantify the effects responsible for a narrow angular distribution with angle dependencies of the velocities for different detection conditions (particles emitted in different directions). Details will be given below.

Dependence on number of pulses per site

As was demonstrated in Chapter 3, one of the most characteristic features of ultrashort pulsed laser ablation of dielectrics, especially sapphire (Al_2O_3) is the occurrence of two

clearly distinguishable ablation regimes [ARV97, TBC89, BrT90]: a ”gentle” ablation in which a few nm in depth are removed per laser shot in a strongly ionized form and which leaves behind a smooth surface and a ”strong” ablation phase characterized by an order of magnitude higher ablation rate per pulse, much lower efficiency in ion production and showing characteristics of ”phase explosion”. This type of behavior was not observed with the conventional ns UV laser pulses [HaI94, RoK84].

An initial experiment was performed to determine the kinetic energy spectrum of the ablation products. The laser parameters were set to: 100 fs pulse duration, 800 nm wavelength, 5 J/cm^2 fluence (above the single-shot ablation threshold), and Al_2O_3 was used as the dielectric target. The laser was at normal incidence and the sample was oriented at 25° with respect to the mass-spectrometer axis, allowing a fixed direction of particle emission during the ablation process. Thus, for this geometry, ablation products are not detected at the maximum emission.

For the conditions used in the present experiments the initial ablation corresponds to the ”gentle” phase, with a low number of pulses per site. Part of the characteristics of this phase has been discussed in Chapter 3.

After a certain number of laser shots the target material has accumulated a sufficiently high density of defects to initiate the ”strong” ablation phase. The crossover occurs after approximately 20 laser shots at 100 fs (see Chapter 3). The discussion will emphasize the differences in the gentle and the strong phase, which correspond to different mechanisms of particle emission.

Velocity distributions for the different atomic species in the ultrashort pulsed laser ablation of sapphire (Al_2O_3) Al^+ and O^+ are shown in Fig. 4.1-2, for normal laser incidence (see Fig. 4.1-1) as a function of number of laser shots. The respective distributions are discussed in terms of fast and slow particles. A first observation is that the different species are spatially separated, according to their mass, due to their different velocities. It is immediately apparent that the most probable velocity of both species decreases as the number of laser shots increases due to the strong onset of a low velocity component in the distribution as the number of shots increases beyond the gentle-to-strong crossover (note that the data have been normalized to the maximum intensity). This is, at first sight, counter-intuitive since there is approximately an order of magnitude more material removed per shot in the strong phase compared to the gentle phase [ARV97] which one would expect to conduct to stronger hydrodynamic effects in the plume, leading to faster and more highly directioned ablated species [Kel90]. Also the surface morphology shows more evidence of a ”violent” material

removal for $N>20$ (Fig. 3.1-1). The data can be reasonably well fitted by single Maxwell-Boltzmann (M-B) distributions when ablation is clearly either within the gentle phase ($N=4$) or the strong phase ($N=100$). For these comparisons we have used 1D M-B fitting functions $(I(v) \propto exp(-m(v-u)^2/2kT))$ with m the mass of the ions and u the flow velocity). We do not want to infer that this is the best fit function to be used for our experiments [ZhG97] but it does seem to be the most appropriate, simple, compromise choice for our experimental conditions. The choice of a one-dimensional Maxwell distribution was motivated also by the fact that the measured quantity is the velocity vector in a well-defined direction.

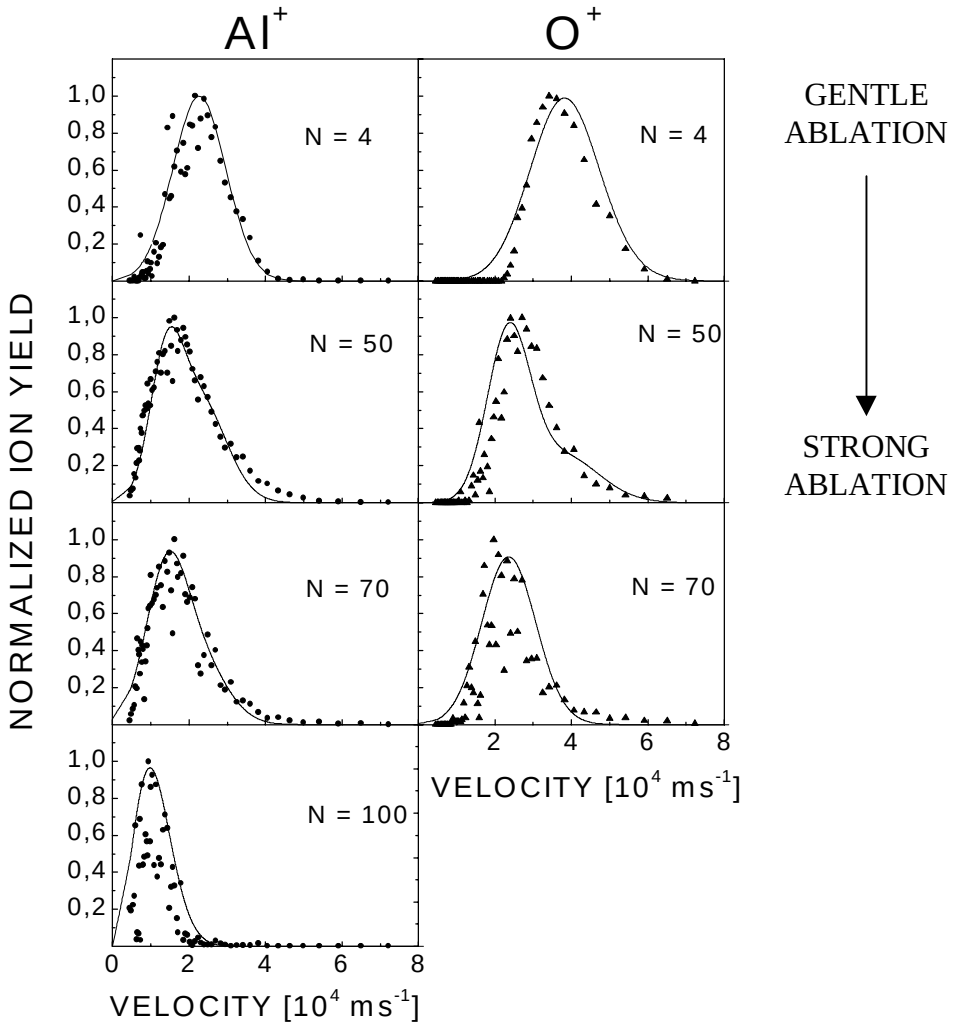

Fig. 4.1-2 Velocity distributions for O^+ and Al^+ ions for different numbers of laser shots per site. Left hand side. Al^+ (circles), right hand side: O^+ (triangles). The Al^+ data are fitted by 1-D Maxwell-Boltzmann distributions (full lines). The full lines on the O^+ plots are the same distributions scaled according to the mass. Experimental conditions: pulse duration-100 fs, laser normal to the sample surface (off-axis detection). See text for details.

The best fits for the Al^+ data are shown in Fig. 4.1-2. The *N=4* distribution has a flow velocity of $u=(2.1\pm0.1)\times10^4$ ms^{-1} and a translational temperature $kT=13\pm1$ eV. The *N=100* data is fitted with a flow velocity $u=10^4$ ms^{-1} and a translational temperature of 5 eV. It is more difficult to satisfactorily fit the intermediate distributions (*N=50,70*). The fits shown in the figure are the sums of two M-B distributions: a slow distribution with $u=1.4\times10^4$ ms^{-1} (kT=8 eV) and a fast distribution that is the same as for N=4 but with decreasing relative intensity as N increases. The calculated distributions shown for O^+ have the same translational temperatures as those fitted to the Al^+ data but the flow velocities have been scaled to give the same value for the momentum, as discussed below. The comparison of the Al^+ fit parameters with the O^+ data is reasonably good for up to N=70 but becomes much worse after this using the momentum scaling (not shown on Fig. 4.1-2 due to low intensities and poor signal to noise ratio for this particular set of data).

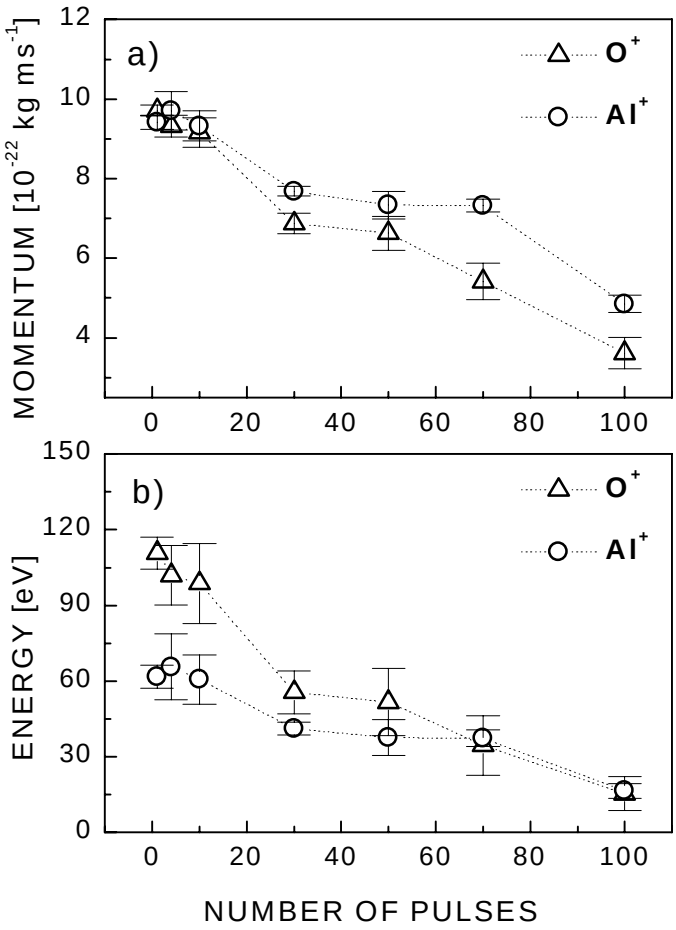

Fig. 4.1-3 Momentum (a) and energy (b) of O^+ and Al^+ species within the plume as a function of number of laser shots. The values were calculated from the measured maxima in the velocity distributions. Circles: Al^+, triangles: O^+. Pulse duration-100 fs, laser normal to the sample surface (off-axis detection).

The maxima of the measured velocity distributions, which are equivalent to the drift velocities *u* from the 1-D M-B fits, have been plotted in Fig. 4.1-3 as both momenta (a) and kinetic energies (b) as a function of the number of shots per site *N*. The values given for O^+ were obtained from separately fitting the experimental data (as discussed for Al^+, above) and not taken from the scaled fits shown in Fig. 4.1-2. This clearly shows that the momenta of the two ablated species (single ionized) are equal for low number of laser shots, i.e. when ablation is "gentle". There is an intermediate range (ca. $20 \leq N \leq 70$) where the most probable velocity corresponds to neither the same momentum nor the same energy. Finally for $N \geq 70$, where ablation is well within the strong regime, accompanied by plasma light emission and crater formation, the ions clearly have the same kinetic energies.

Comparable behavior, with equal momenta for different detected species (chemically different but in the same ionization states) is observed for 25^o laser incidence (ion extraction with grids parallel to the surface). Fig. 4.1-4 and Fig. 4.1-5 demonstrate this for the different masses ($O^{+/2+}$ or Al^+) detected.

We detect a small amount of doubly charged ions (Fig. 4.1-4) contributing 10-15% of the total ion signal. The doubly charged ions have velocities that are twice as fast as the singly charged ions and the momenta scale respectively. This is a further confirmation of the charge scaled momenta the ions obtain due to an impulsive Coulomb explosion from the surface.

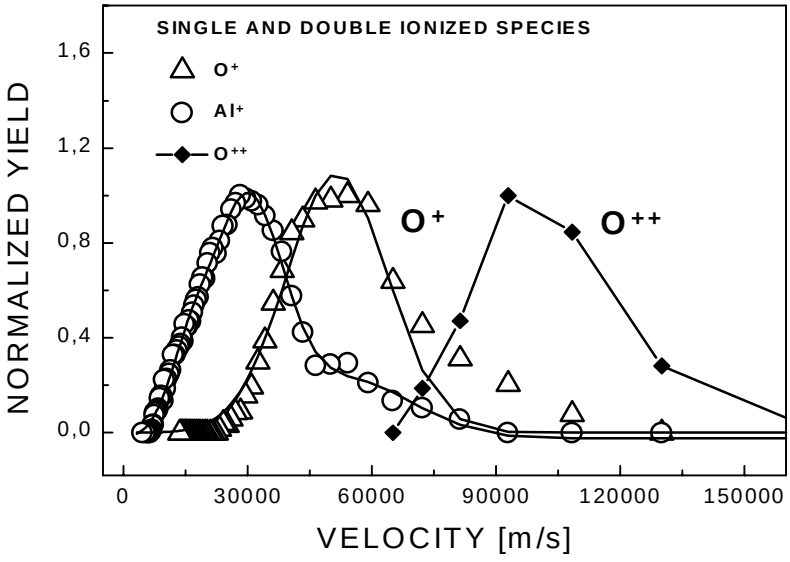

Fig. 4.1-4 Normalized velocity distributions in the gentle phase for Al^+ (open circles), O^+ (open triangles) and O^{2+} (closed diamonds), showing that the doubly charged oxygen ions have twice the velocity of the singly charged ions. TOF normal to surface (on-axis detection), N=2, gentle ablation. Pulse duration-100 fs, fluence 3.9 J/cm^2.

The lack of very highly charged ions and the magnitude of the ion kinetic energies is different from what has been observed in experiments involving sputtering due to the impact of highly charged ions (as discussed above) [ScB96, ChG97]. This is a consequence of the much more homogeneous situation present in the laser experiments rather than a difference in the underlying mechanisms leading to material removal. There is a much more homogeneous charge distribution produced over the entire irradiated area in the laser experiments leading to the removal of the entire upper layers. In highly charged ion experiments the projectile ion strips many electrons from only a few atoms in its path, thus producing a very small region with an extremely high charge density initially surrounded by normal bulk material. This will presumably lead to the explosive removal of a few highly charged ions with correspondingly high kinetic energies.

A similar experiment to the one presented above at 100 fs laser irradiation was performed (for comparison purposes) for a slightly, different pulse duration, namely 200 fs.

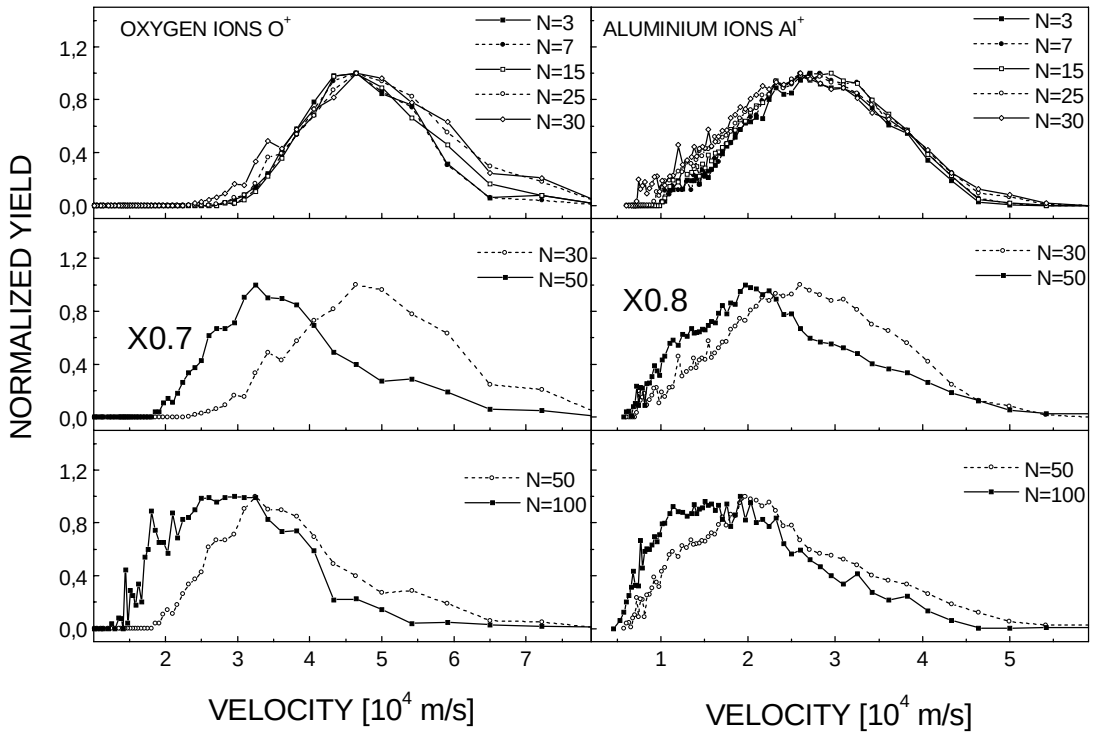

Fig. 4.1-5 Velocity distributions for O^+ and Al^+ from Al_2O_3 (200 fs, 4 J/cm^2) versus N. The distribution is unchanged over the whole gentle phase ($N \leq 30$), then there is a shift at the crossover to the strong ablation phase. A third, lower velocity signal appears for N=100. This marks the stage where a significant crater depth (on the order of the lateral dimensions of the irradiated region) has formed and the plume starts to align along the laser direction. TOF at normal incidence (on-axis detection).

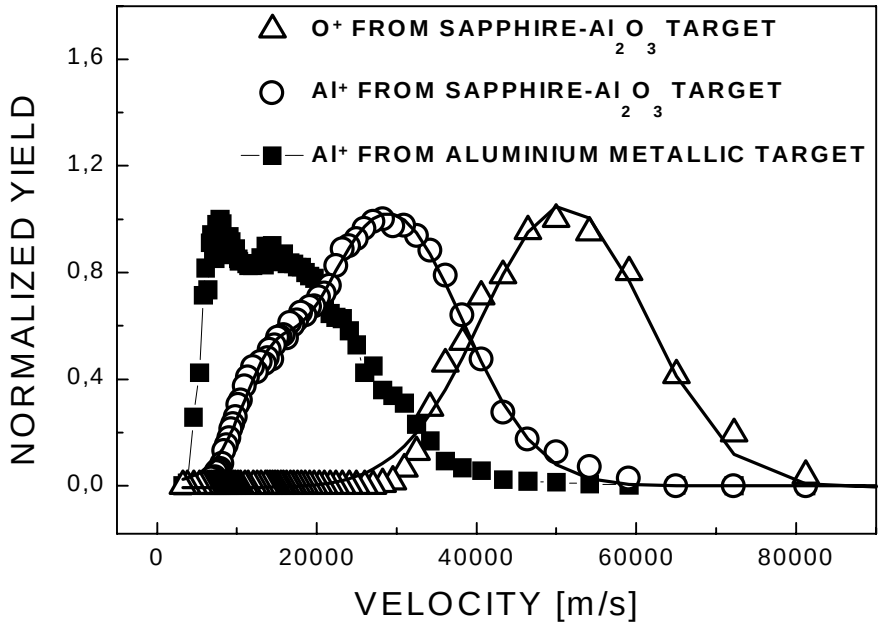

Fig. 4.1-6 Velocity distributions of O^+ and Al^+ from Al_2O_3 (200 fs, N=2, F=4 J/cm^2) and for Al^+ from aluminium metallic target (200 fs, N=4, F=1.1 J/cm^2). On-axis detection.

Velocity distributions of positive ions produced on irradiation with these 200 fs laser pulses at a fluence of 4 J/cm^2 (just above the damage threshold for single shot irradiation ~3 J/cm^2) are shown in Fig. 4.1-5 as a function of the number of laser shots. For the first ca. 30 laser shots at this fluence the velocity distributions are constant. Up to N=30 the ablation can be identified as belonging to the ”gentle” phase with the changeover to ”strong” ablation occurring for higher shot numbers. Beyond N=30 there is a shift in the distributions to lower velocities due to the onset of a low velocity contribution. This shift to lower velocities is accompanied by a change in the morphology of the irradiated surface, a greatly increased roughness and characteristics of a violent removal of material of thermal nature (as has been discussed in the previous chapter and above for 100 fs). This can be clearly seen in the SEM pictures shown in Fig. 3.1-1. An additional low velocity contribution is apparent for N=100 in both the Al^+ and O^+ distributions. This is correlated with the depth of the crater produced on the surface becoming comparable to the lateral dimensions of the irradiated region (it cannot be ruled out that this additional low velocity signal is a consequence of a geometrical effect due to the alignment of the crater parallel to the laser at an angle of 25^o to the surface normal and thus to the axis of the mass spectrometer as evidenced in the case of long channels drilled at non-normal incidence presented in Chapter 6). The trend is very similar to the case of 100

fs pulses irradiation at 5 J/cm^2 (Fig. 4.1-2) [SAR99]. The channel development and alignment along the laser direction will be discussed in Chapter 6.

It is important to note that we observe fast velocity distributions such as those shown in Fig. 4.1-5 for $N \leq 30$ only for dielectric materials with fluences close to the ablation threshold. We have not observed such high velocities for metal or semiconductor targets [SAR99].

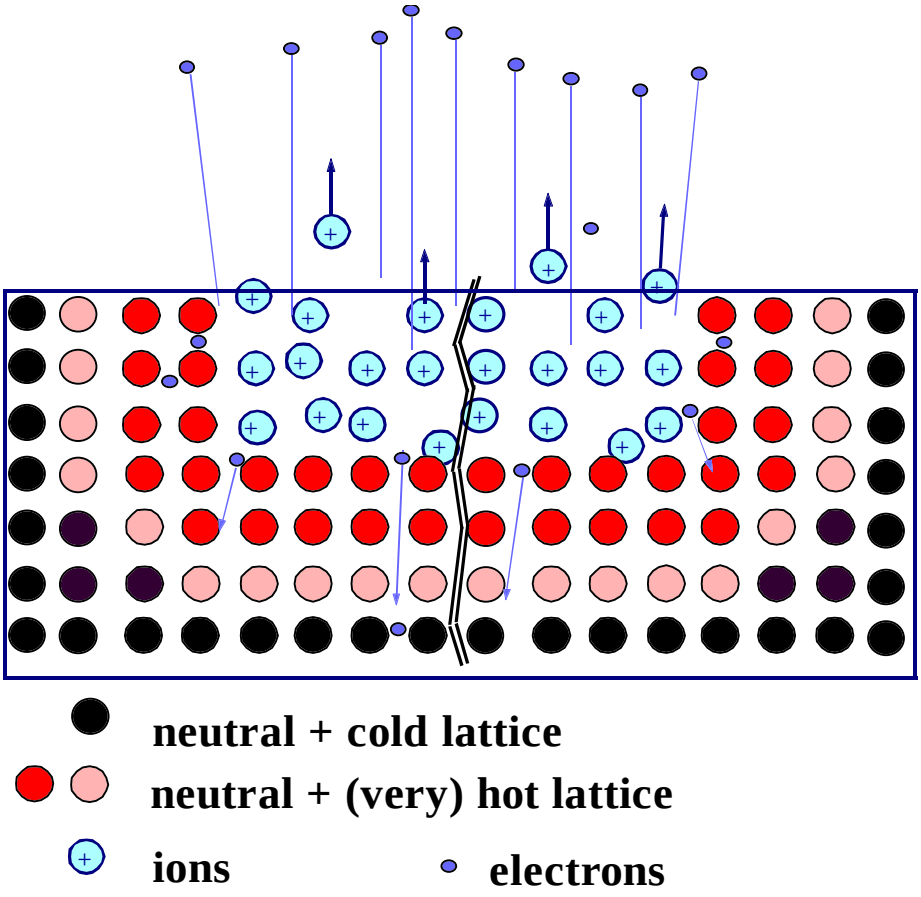

Fig. 4.1-7 Schematic view of a planar Coulomb explosion mechanism for dielectric materials irradiated with ultrashort laser pulses.

This is illustrated in Fig. 4.1-6 where we compare the ion velocity distributions from metallic aluminium and from Al_2O_3. These distributions were measured for N=2 laser shots for sapphire and N=4 for Al metallic sample and normalized to the maximum intensity in the following experimental conditions: 200 fs pulse duration and 4 J/cm^2 for sapphire, respectively 1 J/cm^2 for the metallic sample (both fluences being slightly above the ablation threshold for the respective materials). As clearly evidenced for Al^+ originating from dielectric sapphire the velocity distribution shows a bimodal structure, with a fast peak (energies above 100 eV, depending on the emission angle) followed by a slow peak (less then

50 eV). However, the Al^+ ions from the metal only show the low velocity distribution, similar to that observed from the dielectric after the onset of the ”strong” ablation phase, with high abundance in the “thermal” region of the distribution. The velocity distributions for the dielectric and metallic sample are measured under comparable conditions, i.e. at fluences slightly above the ablation threshold.

The high kinetic energies of the first peak (sapphire sample) are explained in terms of *Coulomb explosion* which is schematically illustrated in Fig. 4.1-7 [FBW65]. These are the consequence of the electrostatic acceleration. The less energetic ions of the second peak will tentatively be attributed to a thermal process, which, especially in the strong etch-phase, resembles *phase explosion* [KeM96, KMM98].

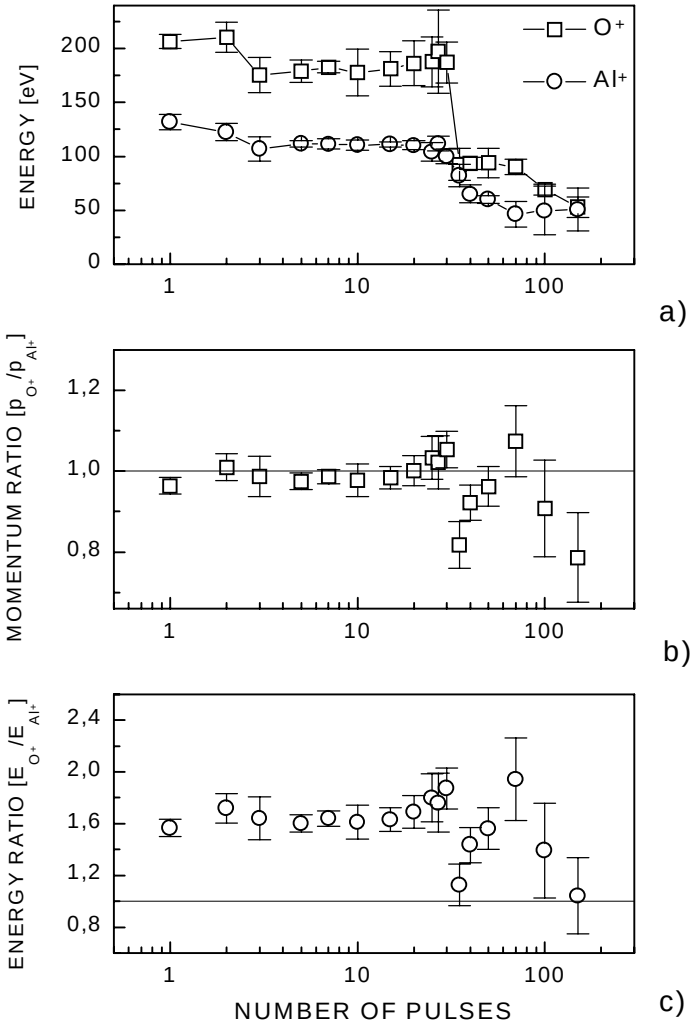

Fig. 4.1-8 a) Kinetic energies of Al^+ and O^+ ions calculated from the maxima of the ion velocity distributions (Fig. 4.1-5). b) Ratio of ion momenta, calculated from maxima of the velocity distributions. c) Ratio of kinetic energies. Laser parameters: 200 fs pulse duration at 4 J/cm^2; on-axis detection.

The maxima of the measured velocity distributions from Al_2O_3 have been converted to kinetic energies and are plotted as a function of the number of laser pulses in Fig. 4.1-8 (a). An abrupt change in the values is apparent at N>30 when the change from ”gentle” to ”strong” ablation occurs. It is also obvious that the velocity distributions measured during the ”gentle” phase do not correspond to the same kinetic energies for the two species emitted from the dielectric. A comparison of the ion momenta immediately shows, as in the case of 100 fs irradiation, that this is the relevant parameter for the low fluence/low *N* behavior as illustrated in Fig. 4.1-8 (b). The momenta of O^+ and Al^+ are equal under the conditions of the gentle phase (the momenta ratio is depicted in Fig. 4.1-8 (b)) After the onset of ”strong” ablation the distributions tend towards values of the same kinetic energies for both ion species Fig. 4.1-8 (c). This tendency is even more accentuated when the average kinetic energy $E_{kin}=m\langle v^2\rangle/2$ is represented. This is depicted in Fig. 4.1-9.

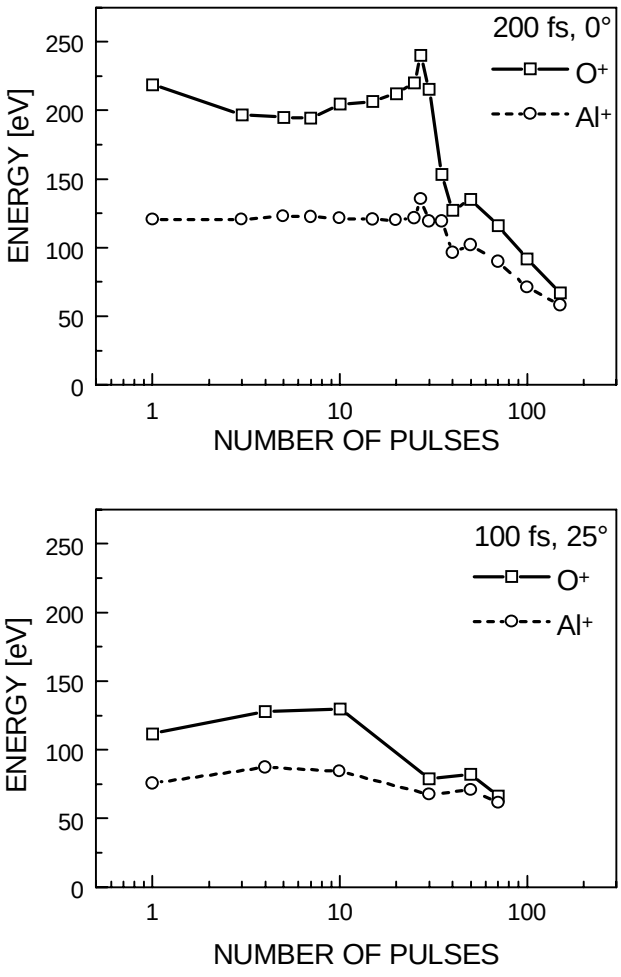

Fig. 4.1-9 Average kinetic energies ($E_{kin}=m\langle v^2\rangle/2$) of Al^+ and O^+ ions as function of number of pulses per site *N* for 200 fs irradiation, on-axis detection (upper panel), and 100 fs irradiation, off-axis detection (bottom panel).

What do these observations suggest? The momenta equality for different masses and the charge scaling of the momenta for different ionization states indicate a non mass-dependent acceleration mechanism with a well-defined momentum transfer as characteristic for a short time electrostatic repulsion. The argumentation is presented below.

Ions of the same momenta for different masses and charge scaled momenta for multiple ionized particles, as observed in the gentle ablation phase would be expected from an impulsive Coulomb explosion from a highly charged surface. The intense laser pulse will induce strong ionization in the surface and underlying regions. The emission of electrons from the surface will leave a high concentration of uncompensated positive charge that will lead to subsequently strong Coulomb repulsion between the ions and to instability of the lattice. For repulsion forces exceeding a certain threshold the ions will be rejected from the surface. The conditions for the development of Coulomb explosion will be detailed later. So, ion emission with high kinetic energies is expected to occur due to charge repulsion. The amount of uncompensated charge will eventually be neutralized either by charge losses in the process of ion ejection, by electron supply from the bulk or by hole diffusion from the irradiated area. The latter processes occur on a much longer time scale for dielectrics than for metals or semiconductors, which is the reason that we are able to observe Coulomb explosion from dielectrics but not for the Al metallic sample. Also retrapping of the slower emitted photoelectrons as a result of surface positive charging cannot be disregarded [PeD77]. The repulsive electric field from the ions at the surface, induced by the laser pulse, will last for a short period of time on the order of 1 ps (as expected from the dynamic measurements presented in the next chapter). The Al^+ and O^+ spend essentially the same time in the action range of this field (nanometer range).

The strength of the electrostatic field is determined by the charge density, which is controlled by the flux of the emitted ions (the charge loss). The electrostatic interaction leading to ion removal is thus many orders of magnitude shorter than the flight time of the ions to the mass spectrometer. Momentum conservation requires that the momenta of the ejected Al^+ and O^+ should be equal under these conditions, i.e. only charge dependent, as observed experimentally. The field is restricted to a definite spatial region (nm) within a definite temporal window (1ps). Thus, the momentum is given by the product of the electrostatic force at the surface due to charge accumulation and the time spent by the particles in the action range of this field (ca. 1 ps) [SAR99].

$$p = \int_0^t q(t')E(t')dt' \qquad \text{E 4.1-1}$$

$$p_{O^+} = p_{Al^+} \qquad \text{E 4.1-2}$$

The minimum charge density at the surface necessary to induce Coulomb explosion can be simply estimated from the condition that the electrostatic stress (force per unit area) has to overcome the local mechanical (or bonding) stress [FBW65].

$$\sigma_{El} \geq \sigma_{Mech} \qquad \text{E 4.1-3}$$

$$\sigma_{El} = \frac{F_{El}}{S} = \frac{f^2 e^2}{\pi^2 \varepsilon a_0^4} \qquad \text{E 4.1-4}$$

$$\sigma_{Mech} = \frac{\Delta l}{l} E \qquad \text{E 4.1-5}$$

For the bulk material the mechanical strength can be estimated by E/10 where E is the Young's modulus of the material (335 Gpa for sapphire) [Pol21, Lid93]. For atoms in the surface layer this will obviously be smaller and we take a compromise average value of E/20 for our estimate. The fractional degree of ionization at the surface, *f*, needed for Coulomb explosion is then given by:

$$f \geq \left(\frac{\pi^2 \varepsilon a_0^4 E}{20 l e^2} \right)^{1/2} \qquad \text{E 4.1-6}$$

where ε is the bulk dielectric constant ($10\varepsilon_o$), a_o is the average atomic spacing in the lattice (2 Å) and l is a factor taking into account the lattice geometry (l=3.64). For Al_2O_3 we obtain f>0.5 (with an estimated error of 50%). f represents the fractional degree of ionization per atom but the meaning could be extended to an overall average ionization degree of the surface. This value of f is consistent with strong acceleration that would also lead to energy values in the range of the observed energies (>100eV).

$$E_{kin} = \frac{m\upsilon^2}{2} = \frac{F_{El}^2 \tau^2}{2m} \qquad \text{E 4.1-7}$$

The overall degree of ionization in the ablated material during the "gentle" phase can be estimated from the volume of the ablated material (measuring the produced crater) and the ion intensities (integrated over velocity and angle and corrected for detection efficiency and amplification) to be approximately 10%. This is considerably less than the 50% estimated above, however, it is exactly what one would expect from considering the results of molecular dynamics simulations [ChG97, HGC97, HGC98]. These simulations have been carried out for

Si and, although there are difficulties with treating the excited electronic states and charge carrier dynamics in a physically realistic way, we believe that the simulations give a qualitatively good picture of the dynamical behavior that can occur, also (perhaps more so) for dielectrics. The simulations showed that the ions are removed from a shallow surface region with the bulk of the material removal occurring later, predominantly as neutral particles, after energy relaxation and heating of the lattice.

The Coulomb Explosion results presented in this chapter (where we are ablating ca. 25 nm per pulse in the gentle phase) suggest that the ions are removed from a surface region with a depth of approximately 2-3 nm, corresponding to roughly 4 lattice parameters, from where the electrons can be efficiently extracted [Hüf95, Hui99]. This shows that the gas-phase effects are non-important within the ion plume during the gentle ablation phase.

No influence of the laser polarization has been noticed on the velocity distributions corresponding to the gentle phase.

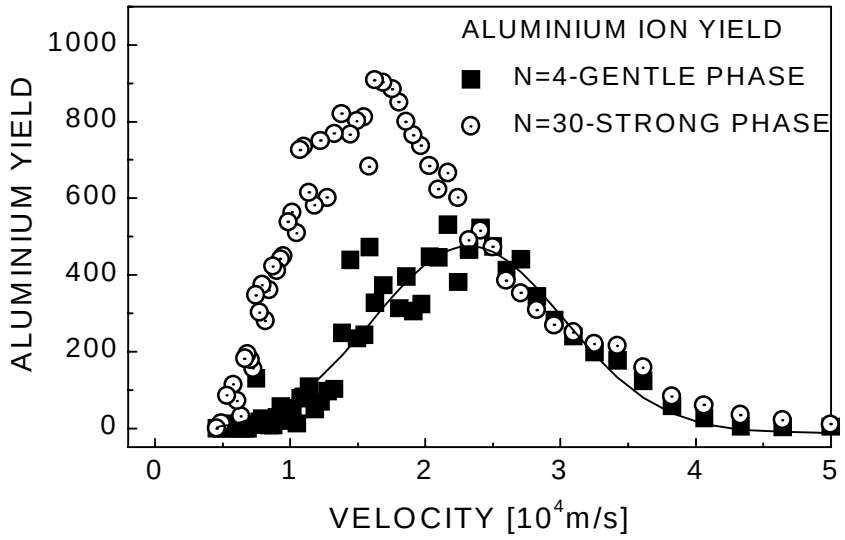

Fig. 4.1-10 Velocity distributions for Al^+ in the gentle (black squares) and strong (open circles) ablation phases showing the absolute ion intensities. Fast ions are still present during the strong ablation but are masked by the strong thermal distribution. (Laser normal to surface, 100 fs at 5 J/cm^2, off-axis detection).

As we have seen, with increasing number of laser shots *N*, the behavior changes noticeably. After approximately 20 shots at 100 fs and 30 shots at 200 fs irradiation, the ablation is much more efficient with up to an order of magnitude more material being removed per pulse. The onset of this ablation phase (initiated by a critical density of defects) has been shown in Chapter 3 to be accompanied by the emission of plasma light from the surface and is characterized by a noticeable shift in the maxima of the velocity distributions of

the ions towards lower values (Fig. 4.1-2, Fig. 4.1-5). Also the morphology of the irradiated spot indicates a violent thermal removal process.

If we return for one moment to Fig. 4.1-6 we notice the presence of a low velocity shoulder in the Al^+ ion velocity distributions for the dielectric material following the fast main peak. The velocity distribution characteristic of the strong phase peak also lies in the same low velocity, "thermal" region. A "thermal" region in the velocity distribution characterizes the small velocity values. These values are too high to be directly linked to a surface temperature as a consequence of the powerful gas-phase effects in the strong phase, which erase the primary information concerning the temperature.

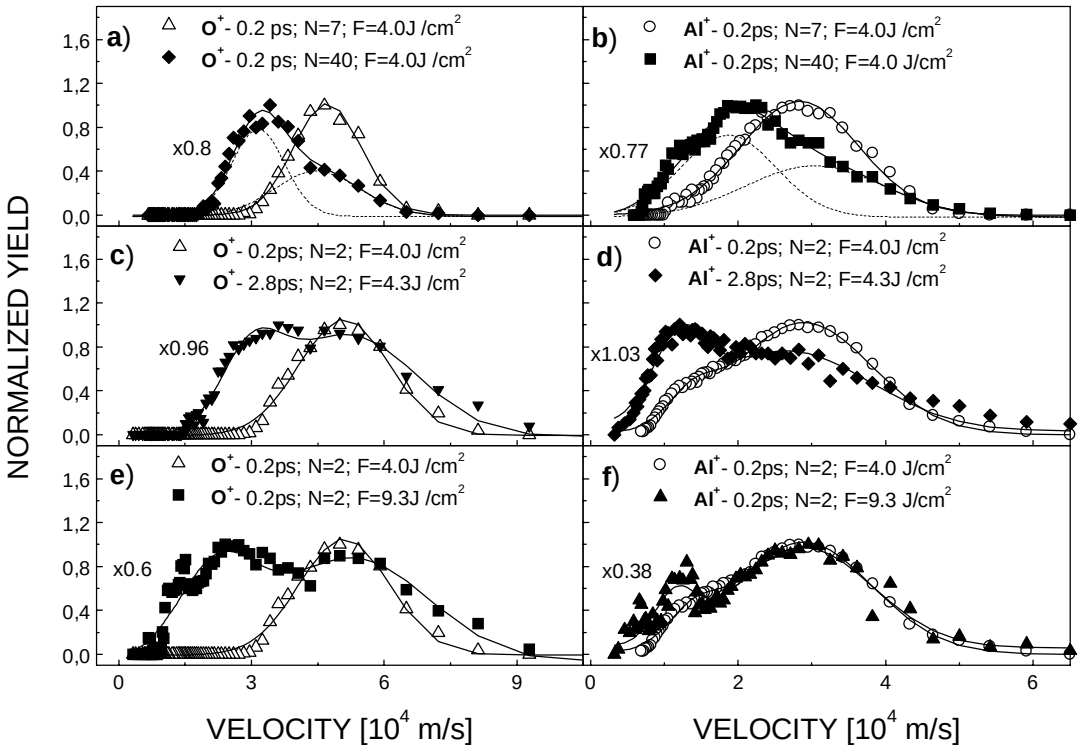

Fig. 4.1-11 The effect of various laser parameters (N, τ, F) on the velocity distributions for O^+ and Al^+. An increase of these parameters enhances the intensity of the slow component regarded as a signature of a thermal effect. The open triangles and circles represent the experimental points for O^+, respectively Al^+ ions for low number of shots (N=2), short pulse duration (200 fs) and low fluence (4 J/cm^2). On-axis detection.

The second slow, broad, shoulder (Fig. 4.1-6) or the strong phase peaks (Fig. 4.1-5) correspond to energies similar to those reported in nanosecond laser ablation of materials (tens of eV) [SiN90, Geo92]. In this case there is a tendency of rather equal energies for the two species then equal momenta. At this point it is difficult to identify unambiguously the mechanisms responsible for the slow peak, but one can at least indicate those that are *not responsible*. One should note that for sub-picosecond pulses an interaction between the laser

and the plume can be disregarded. Also, vaporization can be rigorously excluded, provided it is correct to assume that the vaporization rates for these particular targets are extremely low[1] [KeM98] and there are severe kinetic limitations for normal boiling [MiK99]. The system does not have the time to boil in the classical, thermodynamic sense. This leaves open the probability of phase explosion to occur as the possible thermal mechanism.

If we compare the absolute ion intensities we can see that the fast "Coulomb explosion" ions are still present, as shown in Fig. 4.1-10 where the absolute intensities of the Al^+ velocity distributions have been measured during the gentle and strong ablation phases. However, they are vastly overshadowed by the slow ions in the strong ablation, the “thermal” peak being much more prominent. We have analyzed in Chapter 3 the circumstances of the appearance of a strong phase. There is a strong incubation behavior with previous laser pulses building up an increasing density of defect sites in the target below the ablated region [CAR99]. Strong incubation effects have also been observed in experiments that study the dependence of the ablation threshold on number of laser shots both specifically for Al_2O_3 [ARS99] and for other dielectric materials [ASR2000, VAR96]. The increasing density of defects in the underlying material leads to a much more rapid ionization in the bulk due to lower order absorption from defect sites and an extremely rapid heating of the lattice to a temperature close to the thermodynamic critical temperature. As discussed previously, the main cause of macroscopic laser damage in dielectrics is avalanche ionization [SFR96]. However, this requires a certain free electron density to be initiated. With a gradual build-up of defect density with increasing number of laser shots it becomes increasingly easy, for the same laser fluence, to produce the necessary free electron density for avalanche ionization (via multiphoton absorption from defect states) at an early stage of the ultrashort laser pulse. This therefore leads to a much more efficient coupling of energy into the substrate as the number of laser shots increases. In addition, the defect sites themselves will act as trapping sites strongly coupled to the lattice and contribute to a more efficient energy deposition into the lattice. Thus, although the photoionization may be more intense in the strong phase, we enhance even more the possibility to heat the system to higher temperatures and in an extended depth, given by the defect affected length in contrast to the gentle phase where energy absorption is restricted only to the region with high free electron density. Dense plasma formation, accompanied by clearly observable light emission and an explosive removal of material in a mixture of vapor and liquid droplets is the consequence of this situation characteristic to the strong phase [CAR99, ARV97, TBC89, KeM97]. We interpret the lower velocities and equal kinetic

[1] Assuming a vapor pressure of ~5 atm [KeM98] and a cooling time of 1 ns, the amount of vaporized material

energies observed for $N \cong 100$ in Fig. 4.1-2, Fig. 4.1-5 to be due to ions from the gas-phase ionized vapor plume. These "plasma ions" would be expected to have the same kinetic energy or temperature as a consequence of thermal equilibration in the plume.

Overview of the influence of different laser parameters

Fig. 4.1-11 illustrates the influence of various laser parameters N, τ, F on the velocity distribution. We note the appearance of slow components in the velocity distribution and we attribute these low energy features to a possible thermal behavior as consequence of the target heating. It appears that an increased number of shots, picosecond pulses and high fluences will enhance the probability of thermal effects to occur for reasons that will be discussed below.

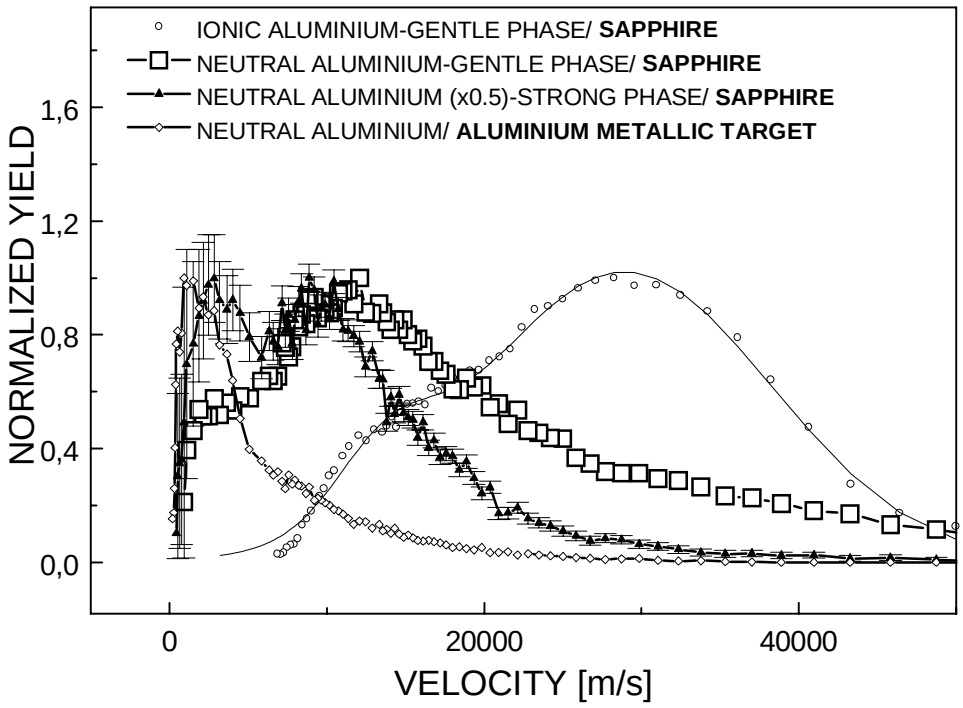

Fig. 4.1-12 Normalized aluminium neutrals-velocity distribution under different conditions of irradiation. N corresponds to the gentle, respectively, strong phase for the sapphire sample, and N=4 for the aluminium metallic sample. Pulse duration: 200 fs, fluence 4 J/cm^2 for sapphire and 1.1 J/cm^2 for aluminium. On-axis detection.

Neutrals time-of-flight studies

Applying a deflection field (1.5 kV in front of the extraction region, see Chapter 2 for details) to remove the ions from the plume and a time delayed ionization source (a XeCl

from Al_2O_3 is ~0.6 nm, as calculated from Eq. E 1.4-3.

excimer laser at 308 nm) for neutral detection it was possible to determine the velocity distributions of the ablated neutral species. These are shown in Fig. 4.1-12 for 200 fs irradiation at 4 J/cm^2.

The XeCl excimer laser was used to ionize the neutral species in the extraction zone. The number of secondary ionized particles are proportional to the number of neutrals present in the extraction region within the focal spot the of XeCl excimer laser. Sapphire samples and metallic aluminium targets have been employed in this experiment.

Obviously, for sapphire, the neutrals arrive much later in the plume in comparison to the early, fast ions from the primary non-thermal, electrostatic mechanism. They have velocities characteristic of the thermal region described above. Small differences have been observed between gentle and strong phases for the dielectric case, but the most probable velocity of Al neutrals from the sapphire target is much higher than the corresponding velocity of the Al neutrals from a metallic Al target (comparison can be made since the laser fluences are in similar relation to the threshold values). This suggests that the temperatures are greatly increased for the laser irradiated dielectrics above the ablation threshold, approaching the critical temperature. No absolute temperature measurements are available but the experimental facts provide evidence for heating to extreme temperatures.

Non-thermal versus thermal mechanisms:

The relative importance of a thermal mechanism in the gentle etch-phase and its significance in the ablation process compared to Coulomb explosion is still unclear. The main ambiguity at this point comes from the inability to correlate directly the ion signal with the total amount of material being removed because of the different ionization efficiencies of the two types of processes. The ion TOF/velocity distribution measurements are sensitive to processes that give a high efficiency of ion production, and therefore will emphasize the Coulomb-explosion mechanism against any possible thermal mechanism, where the information is carried mainly by neutrals. However, based on the combined in-situ (TOF) and ex-situ (SEM) measurements, it is reasonable to believe that for the very first pulses, the Coulomb explosion is the main mechanism of ion emission, while, on increasing *N*, this electrostatic repulsion mechanism for material removal will gradually reduce in importance and thermal mechanisms will dominate up to a violent removal of material associated with phase explosion as we have noticed in Fig. 3.1-7**.**

We can explain this situation with the help of Fig. 3.1-7, Parts (a) and (b). Fig. 3.1-7 shows the *N*-dependence of the total ion yield (integrated over the velocity and angular distribution) corresponding to the peaks previously reported in the gentle and strong ablation

phases and assigned to a dominant Coulomb explosion and to a possible thermal mechanism. The total ion yield (regarded as the sum of the fast ions yield associated with Coulomb explosion and the slow thermal yield) is slowly increasing for *N* corresponding to the gentle ablation with a steep increase at the gentle to strong etch phase crossover and during the strong phase, (where the dominant yield results from the slow, thermal distribution) as a consequence of the augmentation in the ablation rate. The ion yield follows a behavior similar to the ablation rate as seen in [ARV97] and in Fig 3.1-7, but the relative amount of ions (number of ions in the amount of material ablated per pulse) characteristic to the two phases differs significantly, with the ionization efficiency decreasing in the strong etch-phase (Fig. 3.1-7 (c)). As was stated before, the strong phase is the result of incubation with the effect of altering the optical properties and increasing the coupling between the radiation and the target and in the ablation threshold reduction (Fig. 3.2-6-3.2-8) [ARV97]. Fig. 3.2-6 shows the ablation threshold versus *N* for both the sub-ps and ps regimes. The *N*-dependence of the ion yield in Fig. 3.1-7 (we emphasize the dominance of the slow thermal peak during the strong etch-phase as seen in Fig. 4.1-5), ablation threshold (Fig. 3.2-6) and ablation rate (Fig. 3.1-7-b) are related to the degree of incubation, i.e. accumulation of defects induced in the sample.

On increasing *N*, and thus, the degree of incubation by defect formation, the heating efficiency is increased as a consequence of the lower order of absorption and an increased coupling of the laser radiation to the sample [ASR2000]. In this case there may exist the possibility for ***phase explosion*** to occur provided the time scales are appropriate. Assuming that the localization of the energy within the interaction area will last long enough to maintain a high temperature much above the melting temperature, approaching a level of ~0.9 of the thermodynamic critical temperature (T_{tc}), a mixture of vapor and liquid droplets will be violently ejected from the sample [KeM96, ZKG97, MiK99]. Another argument for considering phase explosion is the observation of splashed material traces around the spot rim and the increased number of redeposited particulates, especially after a high number of pulses per site and, hence, altered optical properties. As particles leave the target, a recoil force due to the momentum transfer will act on the surface, leading to a high pressure at the bottom of the crater and forcing the liquid phase out [BaF73, RoK84].

Phase explosion may also be partly responsible for particles in the gentle etch-phase but the small amount of the material being removed and the reduced size of the overheated zone will not allow observable macroscopic droplets to be formed, the material being predominantly expelled in gaseous form. Experiments on different dielectric materials have evidenced the same behavior, fast velocity distributions and charge scaled momenta during

the gentle phase, and a dominance of the thermal aspects in the strong phase, after sufficient incubation occurs with a tendency of equal energies for the ionic species within the plume. In Fig. 4.1-13 the corresponding distributions are presented for the case of a fused silica sample. As observed for the sapphire sample, the fast peak is characteristic only for the dielectric material, while the distribution of Si^+ from a silicon sample belongs merely to the thermal region.

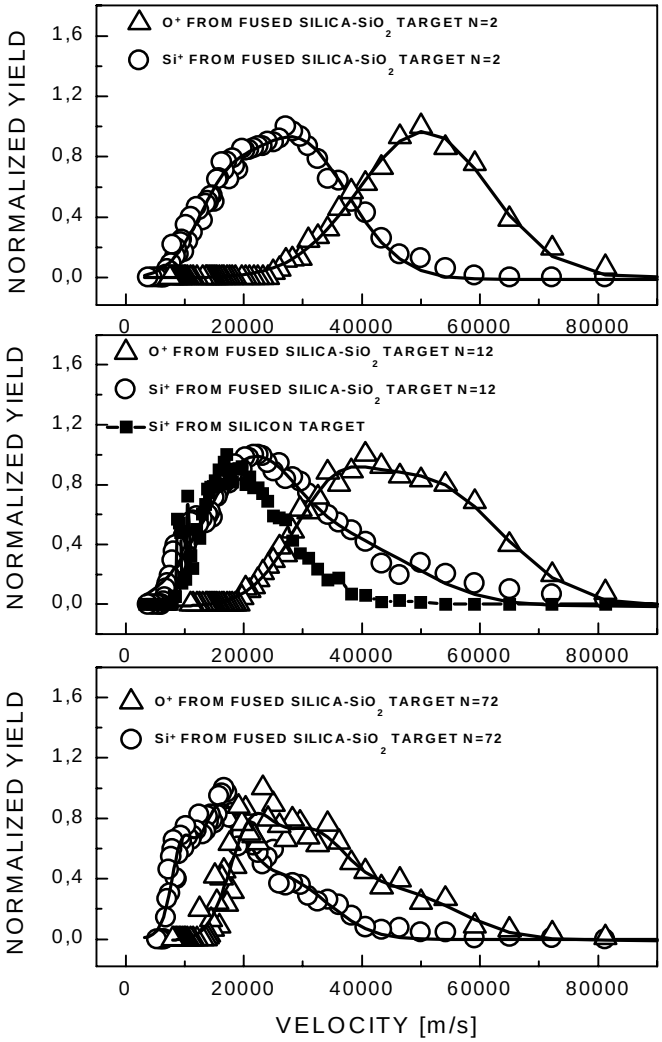

Fig. 4.1-13 Velocity distributions for O^+ and Si^+ ions emitted at 4.3 J/cm^2, 100 fs irradiation of fused silica in the conditions of gentle and strong ablation phases. Si^+ ions from a silicon target are also shown (~1 J/cm^2). On-axis detection.

Angular distribution

Additional arguments to support the underlying thermal nature of the slow distribution can be found from the angular distributions for the two ionic species. They are presented in Fig. 4.1-14 for *N*=4 and *N*=30 pulses per site. The angular distribution (time and velocity

integrated) broadens for the N>30 case ($\cos^3\theta$) due to the contribution of the slow component of the distribution, contrary to the case of N=4 ($\cos^{10}\theta$), corresponding to the gentle etch-phase. In this respect, the total ion yield should be regarded as a superposition of several different ionic components, determined by the presence of different atomic species (i.e. O^+ and Al^+) and a small amount of double ionized species or components derived from different particle emission mechanisms, but fitting with one $\cos^n(\theta)$ distribution describes better the overall broadening effect as a function of the number of pulses per site and allows one to compare angular distributions under different conditions and to characterize them with only one n-parameter which decreases as N increases. The subsequent broadening of the angular distribution while increasing the number of pulses per site will arise from a competition between the mechanism of ejection and the geometry of the crater formed for N>50. Note that the two atomic species O^+ and Al^+ have different masses and, hence different velocities. They travel separately and the instantaneous angular distribution may vary.

Increasing the number of pulses per site the angular distribution of the ion population becomes broader Fig. 4.1-14 (a, b). A possible explanation is a mechanism that involves the explosive ejection of particles, for example phase explosion. Also, due to the round geometry of the crater bottom (for N>50), the particles that are emitted normal to the local surface will lead to a spread in the possible trajectories and to additional collisions inside the crater, subsequently to a broadening of the angular distribution. Also a shifting of the plume towards the laser at a high number of pulses at non-normal incidence is imaginable, especially since our particular experimental set-up rotates the sample and keeps the angle between the TOF detector axis and the laser direction constant (with a non-constant incidence of the laser). However, simulations of the effect of a crater aligned towards the laser direction as well as experimental results at lower number of pulses where no significant crater has formed have ruled out that this effect is responsible for the broader angular distribution in our number of pulses range but it becomes sensitive for N>70. Although the distributions can be related to the mechanisms of particle emission, gas-phase effects cannot be ruled out entirely. Collisions in the expanding plume tend to redistribute the energy and momentum, causing to some extent an overlaying of the information related to the mechanism of expulsion, an effect that is more pronounced in the strong etch-phase.

As the number of pulses is increased, the amount of material increases too (Fig. 3.1-7-b) and the plume undergoes thermalization by collisions. A high number of pulses per site will increase the depth of the crater so that the plume will develop inside the crater and, therefore, be confined in a smaller volume. One should note that in the strong etch-phase, the amount of

material being removed is almost one order of magnitude higher. This will also increase the collision rate and enhance the transfer of energy from different energetic components in the plume. Consequently there will be an additional heating process for the plume inside the crater. The over-pressure attained by the plume being restrained to the crater will also influence the TOF/velocity distribution of the ions. This is a good example of a case where the primary information on the excitation process is being erased by secondary processes [MiK99].

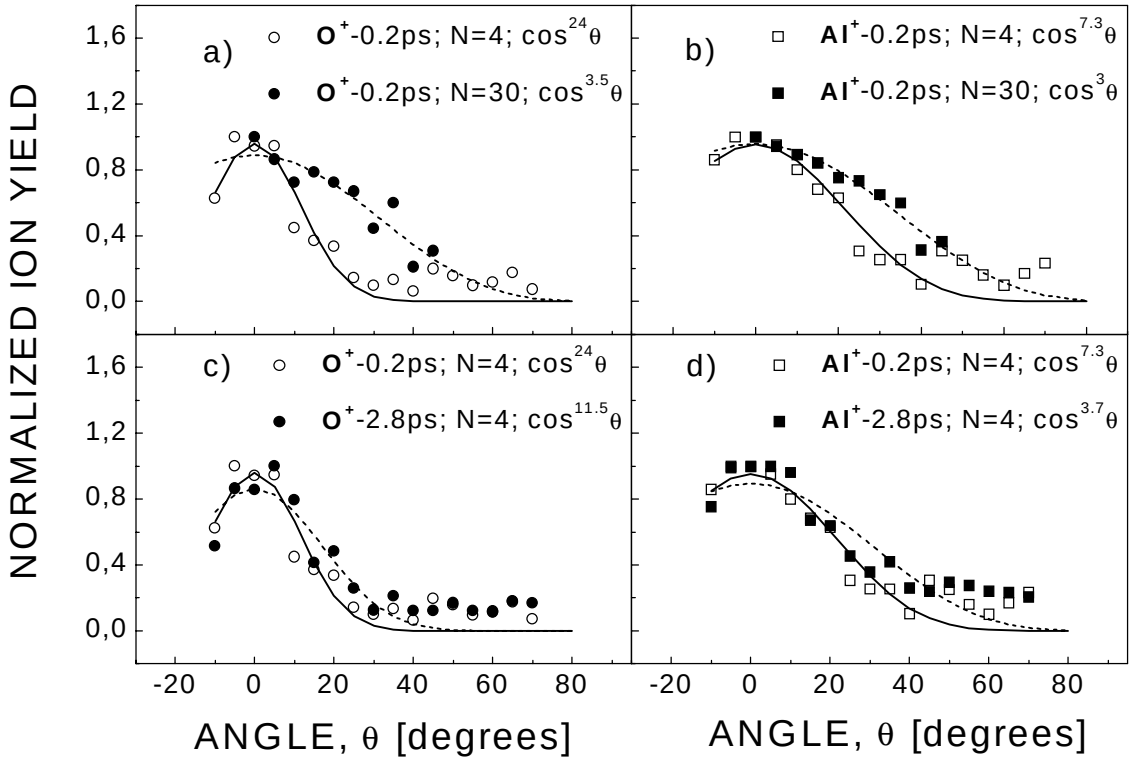

Fig. 4.1-14 The angular distribution of the positive ions (O^+ and Al^+ species) in the plume for different number of pulses per site irradiation (N=4; N=30) (a, b), and for 0.2 ps and 2.8 ps pulse durations (c, d). Laser fluence: 4 J/cm^2 for 0.2 ps and 4.3 J/cm^2 for 2.8 ps irradiation.

Angular distribution measurements have shown also a strong angular dependence in the most probable velocity for the different species, O^+ and Al^+ (Fig. 4.1-15).

In Fig. 4.1-16 we present the TOF distributions with the mass spectrometer working as a simple ion detector without mass resolution recording the ion flux. The signal may be altered by the dependence of the MSP efficiency with the ions energy and electron depletion by secondary emission in the MSP surface, emphasizing the fast particles and diminishing the slow ones, but we find that these traces are useful for species identification giving also an

indication of their temporal history. With the help of a retarding field we were able to discriminate between different components by calculating the cut-off time for a certain stopping voltage which is a direct function of the species mass and charge (in these conditions the kinetic energy should overcome the retarding field and the trace will be depleted when the kinetic energy equals the stopping voltage) and to give a suggestive picture of their behavior under different conditions and especially of their separate flight towards the detector. Noteworthy is the appearance of double ionized species in the strong phase, favored also by the plume confinement in the crater. Picosecond pulses and high fluences also favor double ionized species. The H^+ yield is due to a thin water layer covering the surface, the relative yield of the impurity depending on the laser repetition rate. It was also suggested that H^+ may come from hydroxilated sites [WBJ99].

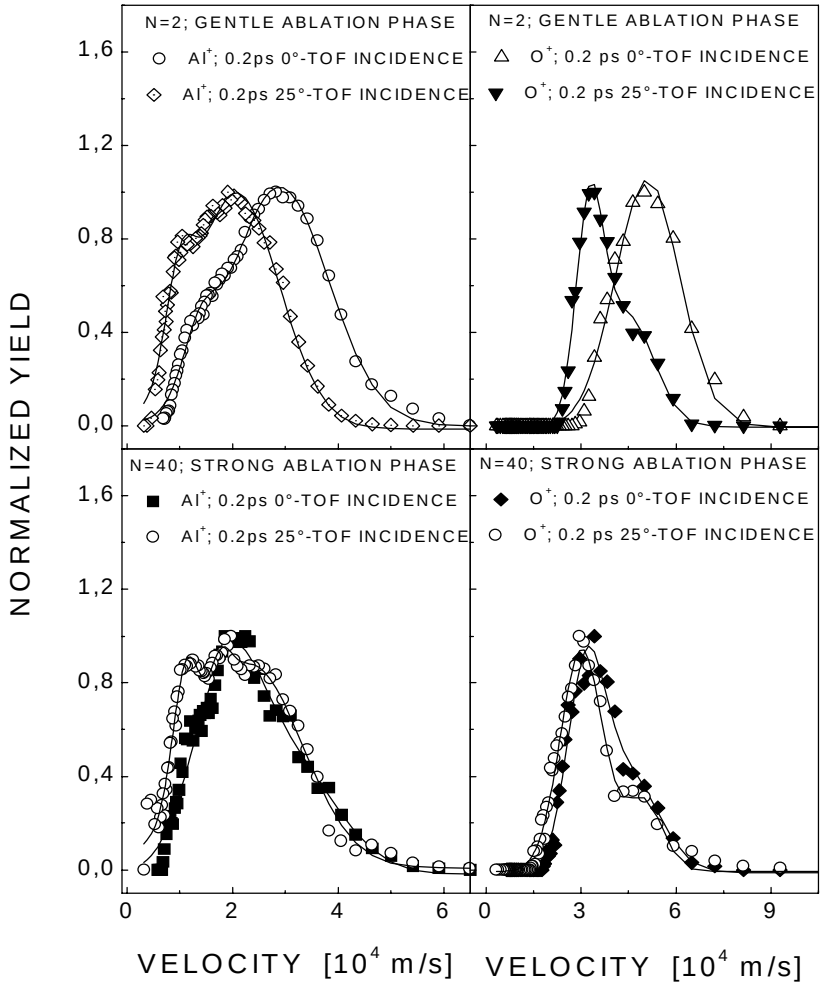

Fig. 4.1-15 Velocity distributions for two angle values of the sample surface normal with respect to the TOF axis, 0° and 25°. The velocities of the distribution maxima are strongly angle dependent, being shifted to lower values when detected at off-axis observation angles.

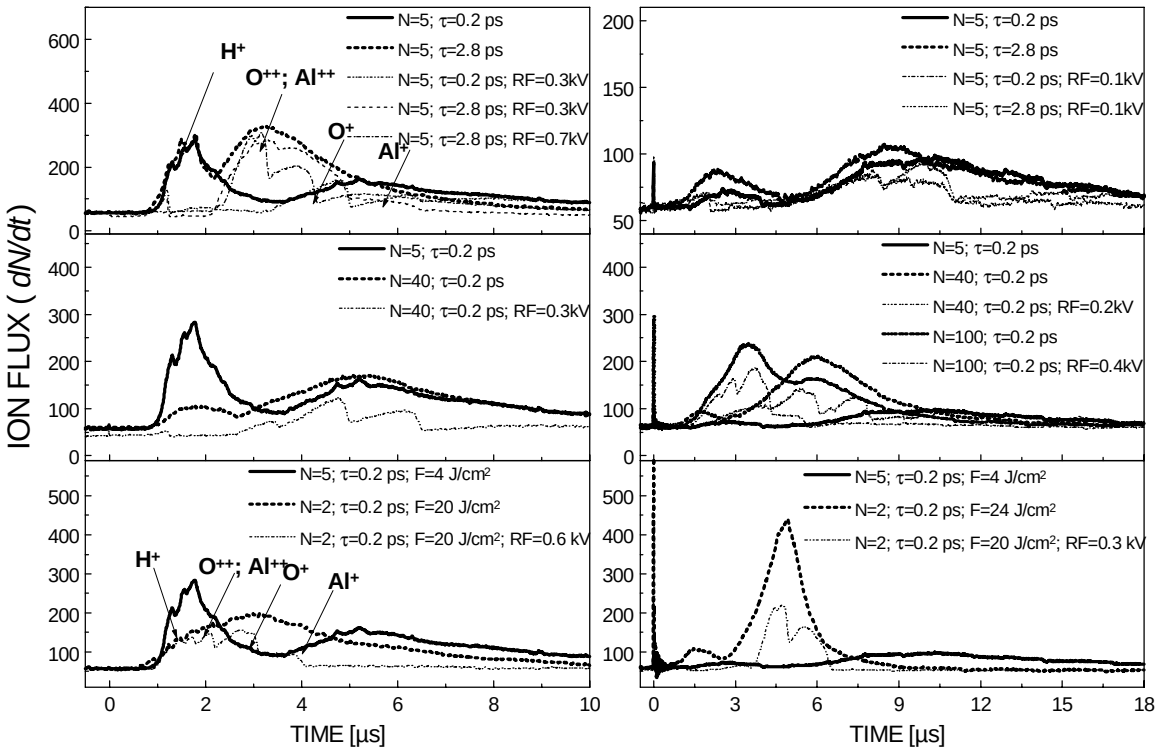

a) TOF axis normal to sample surface

b) TOF axis at 25° incidence

Fig. 4.1-16 Non mass-resolved TOF spectra and the effect of various laser parameters (solid line). The spectra can be resolved with the help of a retarding field. One may note the appearance of double ionized species (dot lines) when one of the following parameters is increased (τ, N, F).

Dependence on pulse duration

The situation becomes more complex as the laser pulse duration is increased to 2.8 ps (F=4.3 J/cm^2, slightly higher than for 200 fs to compensate for the increase in the ablation threshold [ARV97]). Fig. 4.1-17 compares the measured velocity distributions for 200 fs and 2.8 ps pulses where, in both cases, the ablation is clearly in the ”gentle” phase as confirmed by ex-situ investigations of the irradiated areas. The ions produced from ablation with the longer pulses also show the high velocity signals attributed to Coulomb explosion, as discussed above, but there is also a very significant low velocity signal that is generally not observable (or is such a small signal as to be indistinguishable from the fast ions) under ”gentle” phase ablation with 200 fs (or shorter) pulses. This suggests that thermal effects play a greater role when the pulse duration is increased to the ps range due to the onset of electron-phonon coupling energy transfer during the laser pulse for picosecond duration.

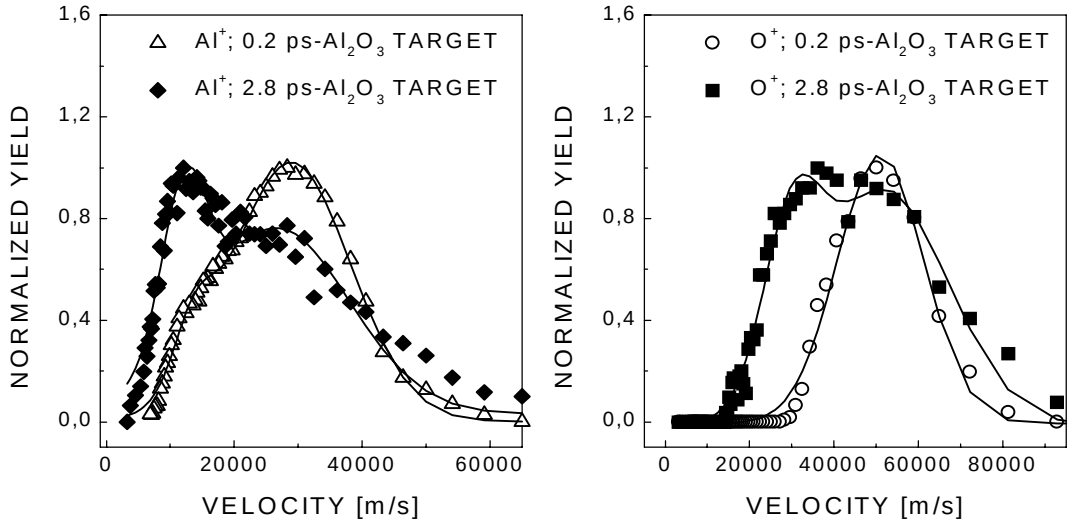

Fig. 4.1-17 Velocity distributions for Al^+ and O^+ at different pulse durations: 0.2 ps and 2.8 ps. Both measurements show the fast Coulomb explosion ion signal but the velocity distributions measured for the longer laser pulses have an additional low velocity signal from ions of thermal origin.

Dependence on laser fluence

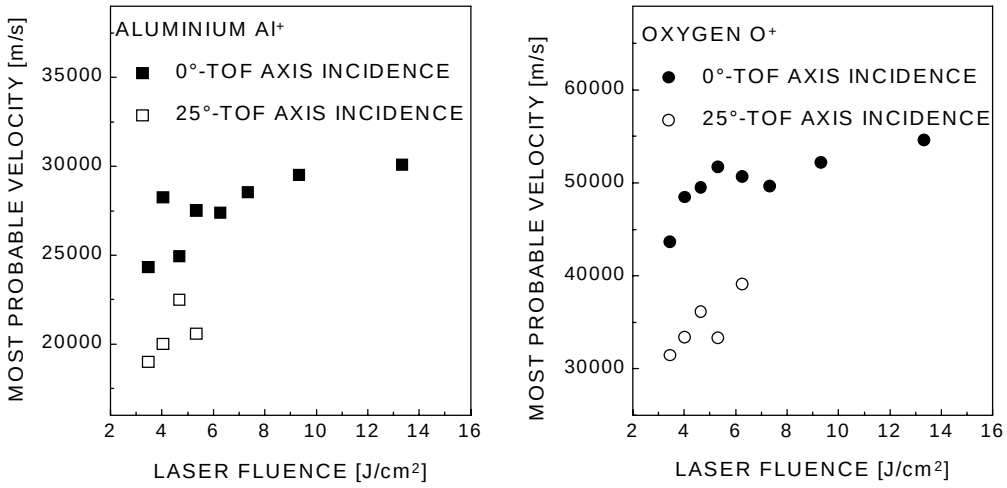

Fig. 4.1-18 Ions' most probable velocity dependence on the laser fluence.

Besides the shift in the balance towards thermal mechanisms while increasing the number of shots/site and pulse duration, we have also shown that increased fluence leads to the appearance of low velocity components in the velocity distributions indicating increasing importance of a thermal mechanism (Fig. 4.1-11-bottom part).

In Chapter 3 it was shown that an effect of the laser fluence is the augmentation in the ablated volume per pulse for both fused silica and sapphire samples which shows saturation at the onset of significant thermal effects. The thermal effects onset can be noticed both in the SEM pictures and in the velocity distributions.

We can also note in Fig. 4.1-18 a slight increase in the most probable velocity extracted from the velocity distributions at different fluences that flattens at about 5-6 J/cm^2, where the surface ionization saturates and stronger thermal effects begin to be present.

4.2 Electron measurements

To obtain additional insight into the processes occurring during the ablation phases, we have measured also the emitted electron characteristics. This can be done by essentially reversing the electric potentials of the TOF spectrometer with suitable values, and negatively biasing the sample. The energy resolution is rather poor since the spectrometer was not designed for this purpose, but the result can be useful for understanding the underlying mechanisms. Clearly, two groups of electrons can be discerned: a very fast contribution (the prompt peak), arriving at the MSP at times less than a μs, corresponding to energies of several eV and a very slow group of ejected electrons, the plume electrons, coming along with the plume at kinetic energies of meV [AAB99]. This can be seen in Fig. 4.2-1 (upper panel), where the two TOF distributions are represented normalized to the individual maxima. The amplitudes are therefore not correlated. The prompt peak has been measured by applying a negative bias on the sample (80 V). Details can be found in Chapter 2. Care was taken that the bias value was not too high to extract the electrons travelling with the plume. Also we can see a clear influence of the laser induced charging on the dielectric surface when we compare the prompt electrons emitted from sapphire with the prompt electrons originating from an Al metallic surface (Fig. 4.2-1-bottom panel), which exhibit higher energies.

The prompt peak is an ablation product since it has a quasi-threshold behavior similar to ion emission (at our apparatus sensitivity). Since this group of electrons obviously reflects the initially emitted photoelectrons, a small electron yield should be detectable at sub-threshold intensities too, with a large increase for electron densities in the conduction band close to the critical density, and, therefore, close to the damage threshold. They originate from direct multiphoton ionization of the valence band electrons and defect states and from additional laser interaction with the free electrons in the conduction band. Daguzan et al. [DGK94] have associated these fast electrons with free carrier absorption in the conduction band. So the yield

is growing extremely fast when the laser intensity exceeds the breakdown threshold due to efficient laser absorption in the high density free electron population, leading to this almost threshold-like behavior. This is illustrated in Fig. 4.2-2. Surface and electron cloud charging effects make quantitative discussions difficult but some conclusions can be inferred.

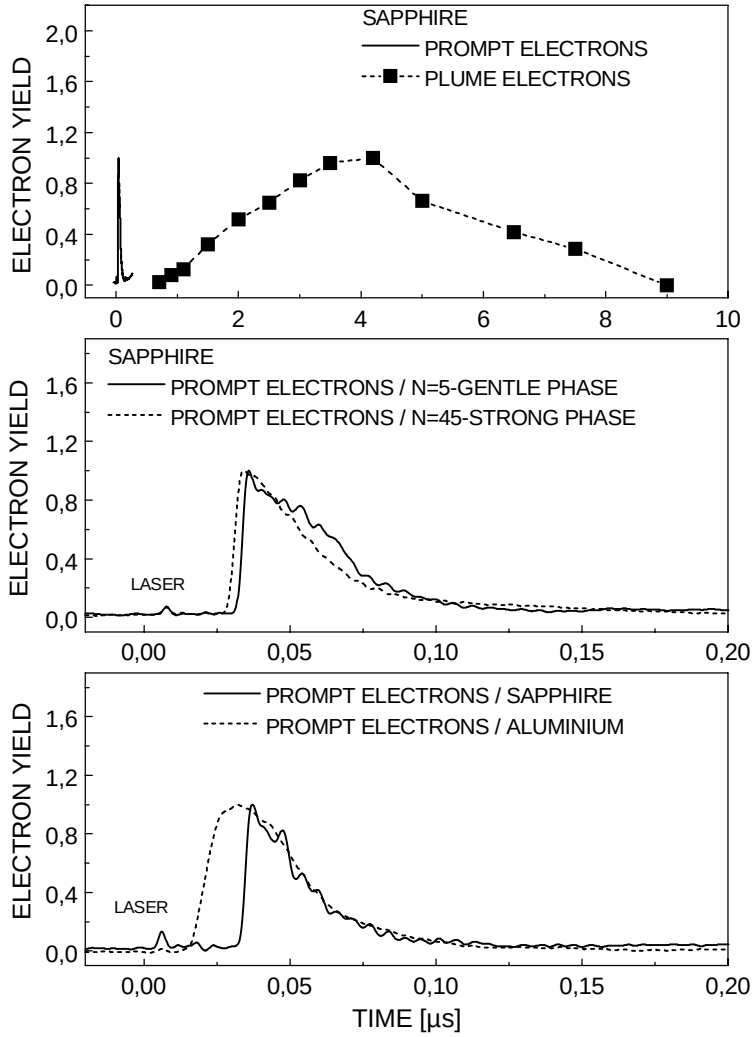

Fig. 4.2-1 Electron TOF distribution for 200 fs, 800 nm laser irradiation of sapphire (at 4 J/cm^2 laser fluence and N=5/45) and metallic aluminium (at 1.1 J/cm^2 laser fluence, N=4). The fast, prompt, electrons and the plume, slow, electrons are visible in the upper panel, The prompt distributions representative for the conditions of gentle (N=5) and strong ablation phases (N=45) for sapphire are also depicted (middle panel). Prompt electrons are responsible for the Coulomb explosion mechanism. Prompt electrons extracted from the dielectric sample have smaller energies compared to the metal case as a consequence of surface charging (on-axis detection).

The prompt electrons appear to be responsible for the Coulomb explosion mechanism. They leave the sample at an early time, which leads to the original build-up of surface charge. The slower electrons (Fig. 4.2-1), travelling with the plume have been measured using a small extraction field, in a procedure similar to the one used for ion recording but with reversed

voltages. Their slow, broad distribution is characteristic for the electrons simply carried along with the plume and help to partially neutralize the latter as it expands. They are a secondary effect of ablation and thus they are unimportant in what concerns the initial ablation mechanisms.

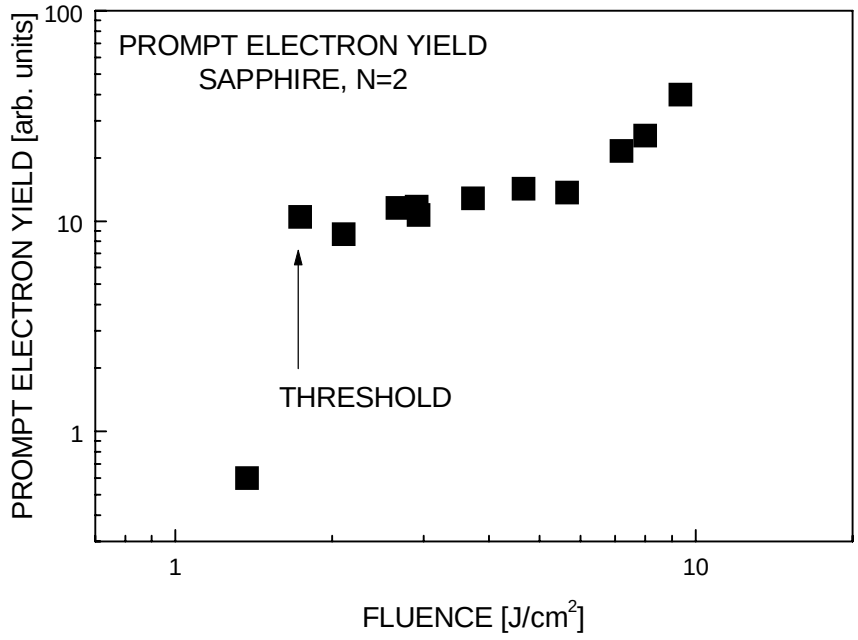

Fig. 4.2-2 Prompt electron yield dependence on the laser fluence. Pulse duration-200 fs, *N*=2.

4.3 Summary

We have discussed the ablation mechanism of dielectrics with emphasis on crystalline Al_2O_3 after laser excitation with pulses of 0.2 and 2.8 ps duration at 800 nm at different number of shots per site and different fluences. We correlated SEM pictures, ion angular distributions, and TOF distributions during and after laser ablation. We propose Coulomb explosion as the principle primary process of particle emission early in the gentle etch-phase, based on mechanistic arguments on momentum considerations, this being in good agreement with the high kinetic energies and high forward-peaking which is observed. Coulomb explosion originates from a strong photoemission with results in prompt electron emission and extreme surface charging

This should be distinguished from the sub-monolayer laser-induced desorption of atoms or ions from excited two-hole states as e.g. observed recently from Si [KIT99] where atoms

are desorbed with a characteristic kinetic energy (in this case 0.06 eV) from an electronically repulsive state at the surface. Such processes are generally site-specific and related to the specific bonding properties of different adatom sites [KnF78, MeG64]. The macroscopic Coulomb Explosion reported here, with the removal of many monolayers per laser shot, leads to much higher kinetic energies on the order of 100 eV with equal momenta for ions of different mass, as would be expected from an impulsive acceleration from a highly charged surface. It is clearly observable under low laser fluence conditions that lead to macroscopic ablation but are not sufficient to induce the formation of a dense plasma as indicated by the low intensity of light observed (mainly scattering from the surface).

Heating becomes significant at a certain degree of incubation and the contribution of Coulomb explosion to the rate of material removal will diminish in favor of a thermal mechanism, although Coulomb explosion was related to ion emission and not directly to the bulk of material removal. Therefore, going to a higher number of pulses for the same laser fluences we observe the transition to a strong etch-phase where the original electrostatic process information is less dominant and explosive thermal effects become more important. Phase explosion is the most likely thermal process involved, since we expect it to be not nearly as kinetically limited as normal vaporization or normal boiling [MGK96]. Also, increasing the laser fluence or the pulse duration will create the conditions for thermal effects to manifest dominantly.

When strong plasma emission is observed optically it is accompanied by the appearance of an intense low velocity component in the ion velocity distributions. For conditions where strong ablation and dense plasma formation are dominant, the kinetic energies of the different ion species tend to be equal, indicating their origin in the decay of the plasma plume.

These results, i.e. the occurrence of different processes, one non-thermal (namely Coulomb Explosion) and the other one thermal (phase explosion) were confirmed by angular distribution measurements, as well as by analysis of the kinetic energy spectrum of emitted neutral particles and electrons.

It was also shown that, besides the influence of increasing the number of shots per site (incubation), also increasing the fluence or pulse duration enhances the thermal effects.